

Loss Terms and Operator Forms of Koopman Autoencoders

25 November 2024

Dustin Enyeart

Department of Mathematics

Purdue University

denyear@purdue.edu

Guang Lin*

Department of Mathematics

School of Mechanical Engineering

Purdue University

guanglin@purdue.edu

Abstract

Koopman autoencoders are a prevalent architecture in operator learning. But, the loss functions and the form of the operator vary significantly in the literature. This paper presents a fair and systemic study of these options. Furthermore, it introduces novel loss terms.

Keywords: Operator learning, Koopman autoencoder, loss function, operator form, neural network, differential equation

1 Introduction

A *neural operator* is a neural network that is intended to approximate an operator between function spaces [1–3]. An example of an output function for a neural operator is a solution to a differential equation. Examples of input functions for a neural operator are the initial conditions or the boundary conditions for the differential equation. The study of neural operators is called *operator learning*.

This paper is about Koopman autoencoders, which is a prevalent neural operator architecture to learn the time evolution of differential equations [4–7]. They are especially popular for dynamic mode decomposition [8–11] and control [12–19]. Other prevalent neural operator architectures are DeepONets [20–25] and Fourier neural operators [25–32].

In the literature, the loss functions and operator forms for Koopman autoencoders vary significantly, and there is not a systematic comparison of them. This chapter presents a fair and comprehensive comparison between loss functions and operator forms for Koopman autoencoders. Furthermore, it introduces novel loss terms that are original to this dissertation.

*Corresponding author

First, Koopman autoencoders are introduced in Section 2. And, the loss functions and operator forms are introduction in Section 3. The differential equations used in this paper are introduced in Section 4. Then, the loss functions and operator forms are introduction in Section 3. Then, large grid-search experiments are presented in Section 5. These experiments are over many combinations for only a small number of epochs. The purpose of these experiments is to identify promising loss functions through robust trends. The purpose of these experiments is to identify robust trends to identify the most promising loss functions. Then, in Section 6, the operator forms and loss functions for the operator forms are compared in more detail. Finally, this paper ends with an overall conclusion in Section 7.

2 Koopman Autoencoders

The Koopman formulation of classical mechanics is an alternative framework of classical mechanics [33–35]. It was inspired by the Hamiltonian formulation of quantum mechanics [36–38]. In this theory, the physical state at a given time is represented as a state in an infinite-dimensional latent space, and an infinite-dimensional operator governs the time evolution in this latent space. Intuitively, the Koopman formulation can be thought of as removing nonlinearity by infinitely increasing the dimension.

The Koopman formulation of classical mechanics can be discretized to provide a numerical scheme by approximating the time-evolution operator by a finite-dimensional matrix K . In this scheme, a physical state s_0 can be evolved into a later physical state s_n by encoding it into the latent space, applying the matrix K repetitively and then decoding it back to the physical space, that is, the equation

$$s_n = R \circ K^n \circ E(s_0)$$

approximately holds, where E is a discretized encoder and R is a discretized decoder. In this numerical scheme, the dimension of this latent space is called the *encoding dimension*.

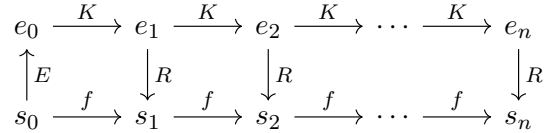


Figure 1: Discretization of the Koopman formulation into a numerical scheme: The physical states at successive time points are denoted by s_0, s_1, \dots, s_{n-1} and s_n . The encoded states at successive time points are denoted by e_0, e_1, \dots, e_{n-1} and e_n . The function f is the true time evolution of the physical state by the time step. The discretized Koopman operator, encoder and decoder are denoted by K, E and R , respectively.

Koopman autoencoders are based on the discretized Koopman formulation where the operator, encoder and decoder are neural networks. The encoder and decoder normally consists of fully connected layers or, sometimes for partial differential equations, convolution layers. And, the operator is a fully connected layer without a bias, and an activation function is not used between successive applications of it. Because the operator is applied repeatedly, it can be useful to use gradient clipping.

3 Loss Functions and Operator Forms

Intuitively, during training, the loss function for the Koopman architecture should regulate three parts. First, the loss function needs to regulate the accuracy of the model, that is, the differences between the predictions and the targets. Second, the loss function should regulate the correspondence between the encoder and decoder because the decoding of an encoding should be the original input. Third, the loss function should regulate the Koopman operator so that it is close to being unitary because the Koopman operator in classical mechanics is a unitary operator. These three types of loss terms are called the *accuracy loss* terms, *encoding loss* terms and *operator loss* terms, respectively.

3.1 Accuracy Loss

The accuracy loss terms measure how well the model predicts the physical states. The accuracy loss terms in this paper are the full accuracy loss, max loss and discounted accuracy loss.

The *full accuracy loss* is the mean squared error between the predictions and the targets, that is, it is the number

$$\frac{1}{n} \cdot \sum_i \|R \circ K^i \circ E(v_0) - v_i\|^2,$$

where K is the Koopman operator, E is the encoder, R is the decoder, n is the number of time steps and v_i is the i -th physical state. This is the most fundamental loss function, and it is what is used for testing.

The *max loss* is the maximum mean squared error between the predictions and the targets, that is, it is the number

$$\max_i \|R \circ K^i \circ E(v_0) - v_i\|^2,$$

where K is the Koopman operator, E is the encoder, R is the decoder and v_i is the i -th physical state [39, 40]. It can be used by itself or with the full accuracy loss to weigh the worse prediction more.

The *discounted accuracy loss* is a weighted mean squared error between the predictions and the targets such that earlier time steps are weighed more. The idea is to prevent the model from getting stuck in at a local minimum such as a steady state. This is an idea from reinforcement learning [41]. In this paper, this is done by weighing the i -th time step by λ^i , where λ is a positive real number that is less than 1. The number λ is called the *discount factor*. Thus, the discounted accuracy loss is the number

$$\frac{1}{n} \cdot \sum_i \lambda^i \|R \circ K^i \circ E(v_0) - v_i\|^2,$$

where K is the Koopman operator, E is the encoder, R is the decoder, n is the number of time steps and v_i is the i -th physical state. This is a generalization of the full accuracy loss in the sense that the full accuracy loss is the discounted accuracy loss with the discount factor 1. The authors are unaware of any papers that use such a loss, that is, it is novel to this paper for the Koopman architecture.

3.2 Encoding Loss

The encoding loss terms restrain the encoder and decoder. Intuitively, the decoding of an encoding should be the original input. The encoding loss terms in this paper are the reconstruction loss, the consistency loss and the metric loss.

The *reconstruction loss* is the mean-square error between the vectors in physical space and their

images after applying both the encoder and the decoder, that is, it is the number

$$\frac{1}{n} \cdot \sum_i \|R \circ E(v_i) - v_i\|^2,$$

where E is the encoder, R is the decoder, n is the number of time steps and each v_i is a vector in the physical space [39, 42]. Intuitively, it encourages the composition of the decoder and the encoder to be the identity. In the numerical experiments in this paper, the physical states were used, but random vectors could also be used.

The *consistency loss* is the mean squared error between the predicted encoded state at a time and the encoding of the target physical state, that is, it is the number

$$\frac{1}{n} \cdot \sum_i \|K^i \circ E(v_0) - E v_i\|^2,$$

where K is the Koopman operator, E is the encoder, n is the number of time steps and each v_i is a vector in the physical space [43]. Intuitively, this together with an accuracy term encourages the compositions of the decoder and the encoder to be the identity.

The *metric loss* is the mean squared error between the squared distances between encoded states and physical states, that is, it is the number

$$\frac{1}{n} \cdot \sum_i \left| \|E(v_i) - E(v'_i)\|^2 - \|v_i - v'_i\|^2 \right|^2,$$

where E is the encoder, each v_i and v'_i are vectors in the physical space and n is the number of vector pairs [13]. In the Koopman formulation of classical physics, the distance between physical states is equal to the distance between their corresponding encoded states. Thus, intuitively, this encourages the structure of the physical states and the geometry of the encoded states to be related.

3.3 Operator Form and Operator Loss

Because the operator in the Koopman formulation is unitary, it is intuitively reasonable to use a loss function that encourages the operator to be unitary. Such a term loss term would measure the failure of the operator to be unitary. The operator loss terms in this paper are the isometry loss, norm loss, unitary loss and determinant loss. Furthermore, because the latent space for Koopman autoencoders is learned, it can be restricted so that its matrix has a certain form in the basis of the latent space. The different operator forms in this paper are the dense form, the tridiagonal form and the Jordan form.

If there is not a restriction on the operator, then all entries of its matrix are learnable parameters. This is the *dense form* of the operator.

Because, a unitary operator is tridiagonal in some basis, the matrix for the operator can be restricted to be tridiagonal, that is, it is of the form

$$\begin{pmatrix} a_1 & b_1 & & & \\ c_1 & a_2 & b_2 & & \\ & c_2 & \ddots & \ddots & \\ & & \ddots & \ddots & b_{n-1} \\ & & & c_{n-1} & a_n \end{pmatrix}$$

where, for each index a_i , b_i and c_i are real numbers. This is called the *tridiagonal form* of the operator. To replicate this structure, a mask can be placed on the operator in the Koopman architecture to make it tridiagonal.

In some basis, a real matrix can be written as a block diagonal matrix where each block is 1×1 or 2×2 of the form

$$\begin{pmatrix} a & b \\ -b & a \end{pmatrix},$$

where a and b are real numbers [44]. This is the *Jordan form* of the operator. In this paper, this is implemented using only 2×2 blocks, that is, the matrix is written in the form

$$\begin{pmatrix} a_1 & b_1 & 0 & 0 & & & & \\ -b_1 & a_1 & 0 & 0 & & & & \\ 0 & 0 & a_2 & b_2 & & & & \\ 0 & 0 & -b_2 & a_2 & & & & \\ & & & & \ddots & \ddots & 0 & 0 \\ & & & & \ddots & \ddots & 0 & 0 \\ & & & & & & 0 & 0 & a_n & b_n \\ & & & & & & & & 0 & 0 & -b_n & a_n \end{pmatrix},$$

where, for each index i , a_i and b_i are real numbers [39]. Intuitively, because this matrix already represents a learned discretized version of a continuous operator, using only 2×2 blocks will be sufficiently expressive because, at worst, it will be expressive of redundant information. Similarly to the tridiagonal restriction, this reduces the number of learnable parameters. Furthermore, this structure

allows for the eigenvalues to be easily computed because the eigenvalues are of the form $a_i + b_i \cdot i$. This is useful in dynamic mode decomposition.

The *norm loss* is the squared distance between the square of the L²-norm of the matrix and 1, that is, it is the number

$$||\|K\|^2 - 1\|^2,$$

where K is the Koopman operator [45]. The intuition of this loss term is that the norm of a unitary operator is 1 [46].

The *isometry loss* is the mean squared error between the squares of the norms of vectors and the squares of the norms of their encodings, that is, it is the number

$$\frac{1}{n} \cdot \sum_i ||\|K(v_i)\|^2 - \|v_i\|^2\|^2,$$

where K is the Koopman operator, n is the number of vectors considered and each v_i is a vector in the physical space. The intuition of loss term is that a unitary operator preserves the norm [46]. This can be done with randomly generated data or with data used for training. In the experiments in this paper, randomly generated data was used.

The *unitary loss* is the mean squared error between $K \circ K^T$ and the identity matrix, that is, it is the number

$$||K \circ K^T - I\|^2,$$

where K is the Koopman operator. The intuition of loss term is that the adjoint of a unitary operator is its inverse [46]. The authors are unaware of any papers that use this loss term, that is, this term is novel to this paper.

The *determinant loss* is the squared distance from the determinant of the Koopman operator to 1, that is, it is the number

$$||\det(K) - 1\|^2,$$

where K is the Koopman operator. The intuition of this loss term is that the determinant of a unitary operator is 1 or -1 [46]. Computing the determinant of a matrix whose size is that of the Koopman operator is usually too computationally expensive for it to be practical. But, if a matrix is tridiagonal, then the determinant is computationally cheap because the determinant of a

tridiagonal matrix

$$\begin{pmatrix} a_1 & b_1 & & & \\ c_1 & a_2 & b_2 & & \\ & c_2 & \ddots & \ddots & \\ & & \ddots & \ddots & b_{n-1} \\ & & & c_{n-1} & a_n \end{pmatrix}$$

can be computed by the formula

$$\det(A_m) = a_m \det(A_{m-1}) - b_{m-1} c_{m-1} \det(A_{m-2}),$$

where A_i denotes the submatrix $A[1:i, 1:i]$ of A . Furthermore, in the Jordan form, the identity blocks on the upper diagonal do not affect its determinant, and the determinant can be computed as if the matrix is tridiagonal. The authors are unaware of any papers that use this loss term, that is, this term is novel to this paper.

For time-reversible differential equation, two koopman operators can be trained where one is for stepping forward through time and the other is for stepping backward through time. Then, a loss term that enforces the inverse operator to be the inverse of the Koopman operator can be implemented. This is called the *reversibility loss* [47]. This loss term is not experimented with in this paper.

3.4 Auxiliary Loss

The *absolute max loss* is the maximum mean squared error between the predictions and the targets across all sample points x_j , that is, it is the number

$$\max_i \max_j \|(R \circ K^i \circ E(v_0))_j - v_{i,j}\|^2,$$

where K is the Koopman operator, E is the encoder, R is the decoder, $v_{i,j}$ is the i -th physical state at the sample point x_j . While the max loss is the maximum mean squared error across the time slices, the absolute max loss is the maximum mean squared error across the time slices and the sample points. The max loss and the absolute max loss are the same for ordinary differential equations, but they are different for partial differential equations. By itself, in practice, the absolute max loss is not enough to be an accuracy loss, but it can be useful together with another accuracy term. Intuitively, it penalizes the most extreme errors. The authors are unaware of any papers that use this loss term, that is, it is novel to this paper.

Physics-informed loss terms are terms that encourage the model to obey the laws of physics [48, 49]. An example is enforcing the model to conserve energy in systems where energy is conserved, such as for simple harmonic motion, the pendulum or wave equation. Another example of a physics-informed loss term is enforcing Gauss’s laws in electromagnetism. The energy-conservation loss is experimented with in the numerical experiments for the pendulum.

4 Differential Equations

This section introduces the differential equations that are used for the numerical experiments in this paper. The ordinary differential equations are the equation for simple harmonic motion, the equation for the pendulum, the Lorenz system and a fluid attractor equation. The partial differential equations are the wave equation, the heat equation, Burger’s equation and the Korteweg-de-Vries equation.

4.1 Simple Harmonic Motion

The equation for *simple harmonic motion* is the differential equation

$$\frac{d^2x}{dt^2} = -x.$$

This is a time-dependent second-order linear ordinary differential equation whose dimension is 1. This equation is used to model a mass on a spring, where the variable x is the displacement of the mass from its equilibrium position.

In the numerical experiments in this paper, the models attempt to learn the solution to this differential equation as a function of the initial condition. To get data, initial positions are generated randomly. Then, this differential equation is numerically solved for these initial conditions using the Runge-Kutta Method [50].

4.2 Pendulum

The equation for the *pendulum* is the differential equation

$$\frac{d^2\theta}{dt^2} = -\sin(\theta).$$

This is a time-dependent second-order nonlinear ordinary differential equation whose dimension is 1. This equation models the motion of a pendulum in a constant gravitational field, where the variable θ is the angle of the pendulum from vertical.

In the numerical experiments in this paper, the models attempt to learn the solution to this differential equation as a function of the initial condition. To get data, initial positions are generated randomly. Then, this differential equation is numerically solved for these initial conditions using the Runge-Kutta Method [50].

4.3 Lorenz System

The *Lorenz system* is the differential equation

$$\begin{cases} \frac{dx}{dt} = y - x \\ \frac{dy}{dt} = x - x \cdot z - y \\ \frac{dz}{dt} = x \cdot y - z. \end{cases}$$

This is a time-dependent first-order nonlinear ordinary differential equation whose dimension is 3. Historically, this equation was used in weather modeling. Now, it provides a benchmark example of a chaotic system.

In the numerical experiments in this paper, the models attempt to learn the solution to this differential equation as a function of the initial condition. To get data, initial positions are generated randomly. Then, this differential equation is numerically solved for for these initial conditions using the Runge-Kutta Method [50].

4.4 Fluid Attractor Equation

The differential equation

$$\begin{cases} \frac{dx}{dt} = x - y + x \cdot z \\ \frac{dy}{dt} = x + y + y \cdot z \\ \frac{dz}{dt} = x^2 + y^2 + z \end{cases}$$

is used to model fluid flow around a cylinder [51]. It is a time-dependent first-order nonlinear ordinary differential equation whose dimension is 3.

In the numerical experiments in this paper, the models attempt to learn the solution to this differential equation as a function of the initial condition. To get data, initial positions are generated randomly. Then, this differential equation is numerically solved for for these initial conditions using the Runge-Kutta Method [50].

4.5 Heat Equation

The *heat equation* is the differential equation is

$$\frac{\partial u}{\partial t} = \frac{\partial^2 u}{\partial x^2}.$$

This equation is a time-dependent first-order linear partial differential equation whose range dimensions are both 1. It is used to model heat flow.

In the numerical experiments in this paper, the models attempt to learn the solution to these differential equations as a function of the initial condition. Furthermore, Dirichlet boundary conditions are used for these equations such that the value of the unknown function is 0 on the boundary. To get data, initial conditions are made by generating random symbolic expressions that satisfy the boundary conditions, and these expressions are then numerically sampled. Then, the partial differential equation is numerically solved for these initial conditions [52].

4.6 Wave Equation

The *wave equation* is the differential equation is

$$\frac{\partial^2 u}{\partial t^2} = \frac{\partial^2 u}{\partial x^2}.$$

This equation is a time-dependent second-order linear partial differential equation whose range dimensions are both 1. It is used to model waves on strings.

In the numerical experiments in this paper, the models attempt to learn the solution to these differential equations as a function of the initial condition. Furthermore, Dirichlet boundary conditions are used for these equations such that the value of the unknown function is 0 on the boundary. To get data, initial conditions are made by generating random symbolic expressions that satisfy the boundary conditions, and these expressions are then numerically sampled. Then, the partial differential equation is numerically solved for these initial conditions [52].

4.7 Burger's Equation

Burger's equation is the differential equation

$$\frac{\partial u}{\partial t} = \frac{\partial^2 u}{\partial x^2} - u \frac{\partial u}{\partial x}.$$

This is a time-dependent first-order nonlinear partial differential equation whose domain dimension and range dimension are both 1. It is used to model some fluids.

In the numerical experiments in this paper, the models attempt to learn the solution to this differential equation as a function of the initial condition. Furthermore, Dirichlet boundary conditions are used for this equation such that the value of the unknown function is 0 on the boundary. To get data, initial conditions are made by generating random symbolic expressions that satisfy the boundary conditions, and these expressions are then numerically sampled. Then, the partial differential equation is numerically solved for these initial conditions [53].

4.8 Korteweg-de-Vries Equation

The *Korteweg-de-Vries equation*, which is abbreviated as the *KdV equation*, is the differential equation

$$\frac{\partial u}{\partial t} = 6u \frac{\partial u}{\partial x} - \frac{\partial^3 u}{\partial x^3}.$$

This is a time-dependent first-order nonlinear partial differential equation whose domain dimension and range dimension are both 1. It is used to model some fluids.

In the numerical experiments in this paper, the models attempt to learn the solution to this differential equation as a function of the initial condition. Furthermore, periodic boundary conditions are used for this equation, that is, the value of the unknown function is the same on each endpoint of the spatial domain. To get data, initial conditions are made by generating random symbolic expressions that satisfy the boundary conditions, and these expressions are then numerically sampled. Then, the partial differential equation is numerically solved for these initial conditions [54].

5 Large Grid Searches

The experiments in this section are grid searches that cover a large number of combinations for a only a small number of epochs. The objective of these numerical experiments is to find robust trends in the choice of loss terms and options. This is done by analyzing mean effects, the best combinations and direct comparisons.

For each numerical experiment, minimal preliminary testing was performed to find reasonable parameters of the model, such at its size. Then, these parameters were fixed for the experiment. This is to prevent bias towards the loss functions that are novel to this paper.

In this section, the dense form and tridiagonal form of the operator are considered, but the Jordan form is not considered. The Jordan form of the operator is considered in the next section.

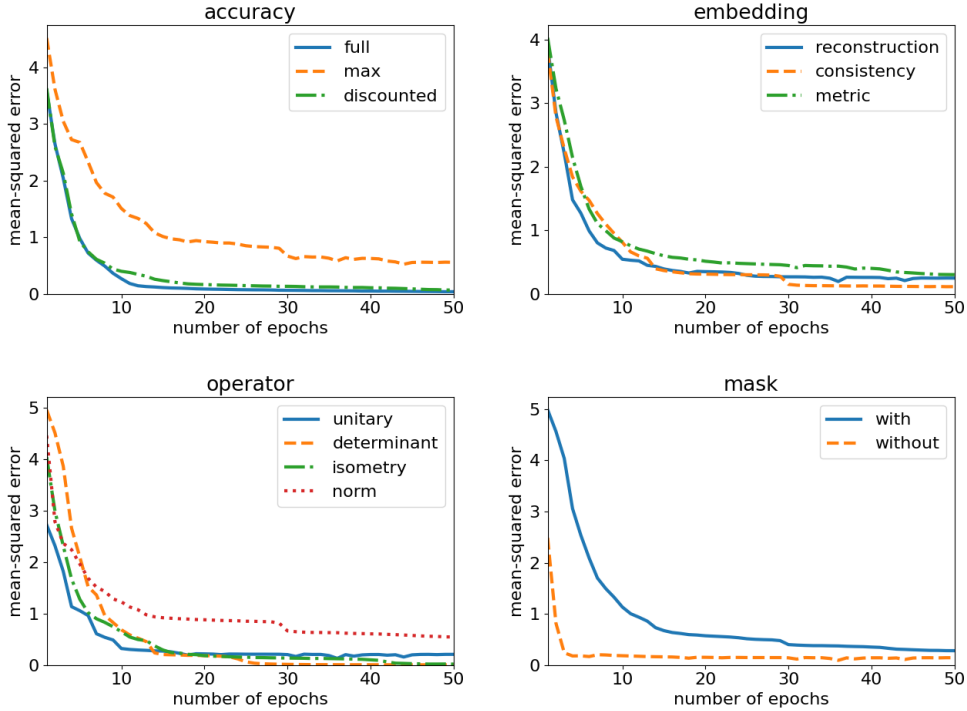


Figure 2: The mean effect of the different options of the numerical experiment for simple harmonic motion. The top left plot compares the mean effect of the different accuracy loss terms. The top right plot compares the mean effect of the different embedding loss terms. The bottom left plot compares the mean effect of the different operator loss terms. The bottom right plot compares the mean effect of whether or not a mask is used.

5.1 Simple Harmonic Motion

In this numerical experiment, the embedding dimensions 16, 32 and 64 were considered. Furthermore, all combinations between the accuracy loss terms, the embedding loss terms, the operator loss terms, and whether or not a mask was used so that the operator is tridiagonal were considered, except that the determinant loss is only considered with a mask. Thus, 216 combinations were considered. Figure 2 shows the mean error for the different options as the number of epochs increases. Table 1 shows the ten best combinations at 20 epochs. Table 2 shows the mean relative times for the different options, that is, the mean times for the different options divided by the overall mean time. Figure 3 is direct comparisons between the accuracy terms and also the embedding terms.

For the accuracy loss terms, on average, the full accuracy loss and the discounted accuracy loss

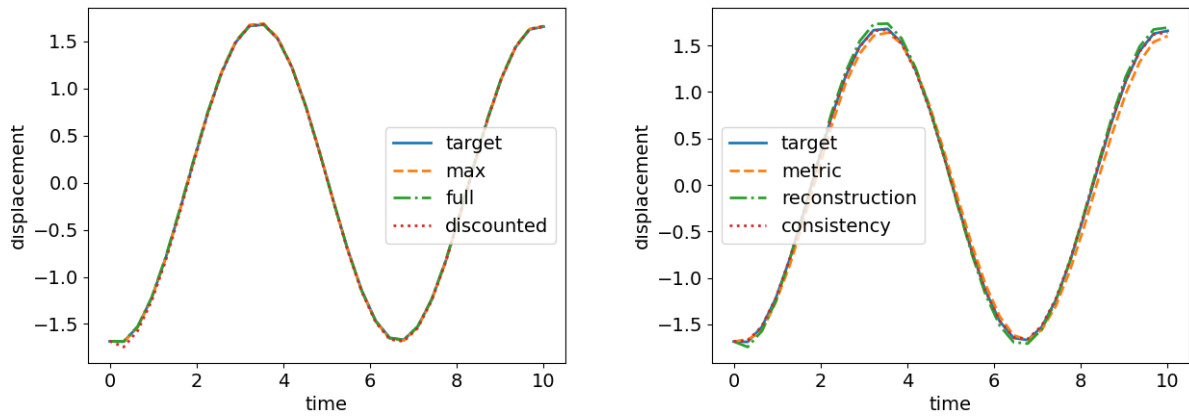


Figure 3: Direct comparison of loss terms for the simple harmonic motion. On the left, the accuracy term is varied while the other terms are fixed. On the right, the embedding term is varied while the other terms are fixed. In each comparison, the embedding dimension is 64, a mask is used, the determinant loss is used, and an auxiliary loss term is not used. In the comparison of the accuracy terms, the reconstruction loss is used. In the comparison of the embedding terms, full accuracy loss is used.

Table 1: The ten best combinations for the numerical experiment for simple harmonic motion at 20 epochs. The dimension is the dimension of the latent space.

error	accuracy	embedding	operator	mask	dimension
0.000306	full	reconstruction	unitary	with	64
0.000318	full	reconstruction	determinant	with	16
0.000515	discounted	reconstruction	unitary	with	32
0.000535	max	reconstruction	unitary	with	64
0.000543	discounted	reconstruction	determinant	with	32
0.000575	full	reconstruction	determinant	with	32
0.000586	max	reconstruction	determinant	with	16
0.000668	full	reconstruction	determinant	with	64
0.000729	discounted	reconstruction	unitary	with	64
0.000733	full	reconstruction	unitary	with	16

performed about the same. They both performed significantly better than the maximum accuracy loss. Five of the best ten combinations used the full accuracy loss, three used the discounted accuracy loss, and two used the maximum accuracy loss. In the direct comparison, all the accuracy loss terms performed similarly.

For the embedding loss term, on average, the three loss terms performed about the same. The metric loss performed slightly worse than the reconstruction loss and the consistency loss. But, all of the best ten combinations used the consistency loss. In the direct comparison, the consistency loss does slightly better than the other embedding loss terms.

For the operator loss term, on average, the isometry loss, the unitary loss and the determinant loss performed similarly, and these three terms performed significantly better than the norm loss. Five of the best ten combinations used the unitary loss and five used the determinant loss.

For the mask, on average, having as mask performed much better. Furthermore, all of the best ten combinations used a mask.

Some of the same combinations of options with different embedding dimensions appeared in the best ten combinations. This demonstrates that these loss combinations are robust.

Table 2: The mean relative times for the numerical experiment for simple harmonic motion.

option	mean time
full	1.033703
max	0.932336
discounted	1.033961
reconstruction	1.127289
consistency	1.023493
metric	0.849218
unitary	0.994508
determinant	1.178594
isometry	0.899820
norm	1.016375
with	1.038539
without	0.948614

Table 3: The ten best combinations for the numerical experiment for the pendulum at 40 epochs. The dimension is the dimension of the latent space.

error	accuracy	embedding	operator	auxiliary	mask	dimension
0.028013	discounted	reconstruction	determinant	energy	with	64
0.028057	full	reconstruction	unitary	none	with	32
0.029205	discounted	reconstruction	isometry	energy	without	64
0.030154	full	reconstruction	unitary	energy	with	32
0.031289	max	reconstruction	determinant	none	with	64
0.031841	max	reconstruction	unitary	none	with	64
0.032055	discounted	reconstruction	isometry	none	without	64
0.032307	discounted	reconstruction	unitary	none	with	32
0.032504	full	reconstruction	unitary	none	with	64
0.032866	full	reconstruction	isometry	energy	without	64

For the most part, the mean times for the options are similar. The reconstruction loss performed slightly slower than the other embedding loss terms. And, the determinant loss term performed slightly slower than the other operator loss terms.

5.2 Pendulum

In this numerical experiment, the embedding dimensions 32 and 64 were considered. Furthermore, all combinations between the accuracy loss terms, the embedding loss terms, the operator loss terms, whether or not the auxiliary energy-conservation loss term was used and whether or not a mask was used so that the operator is tridiagonal were considered, except that the determinant loss is only considered with a mask. Thus, 288 combinations were considered. Figure 4 shows the mean error for the different options as the number of epochs increases. Table 3 shows the ten best combinations at 40 epochs. Table 4 shows the mean relative times for the different options, that is, the mean times for the different options divided by the overall mean time. The energy-conservation loss term is implemented by using

$$\frac{1}{2} \frac{d\theta}{dt} + (1 - \cos(\theta))$$

as the energy.

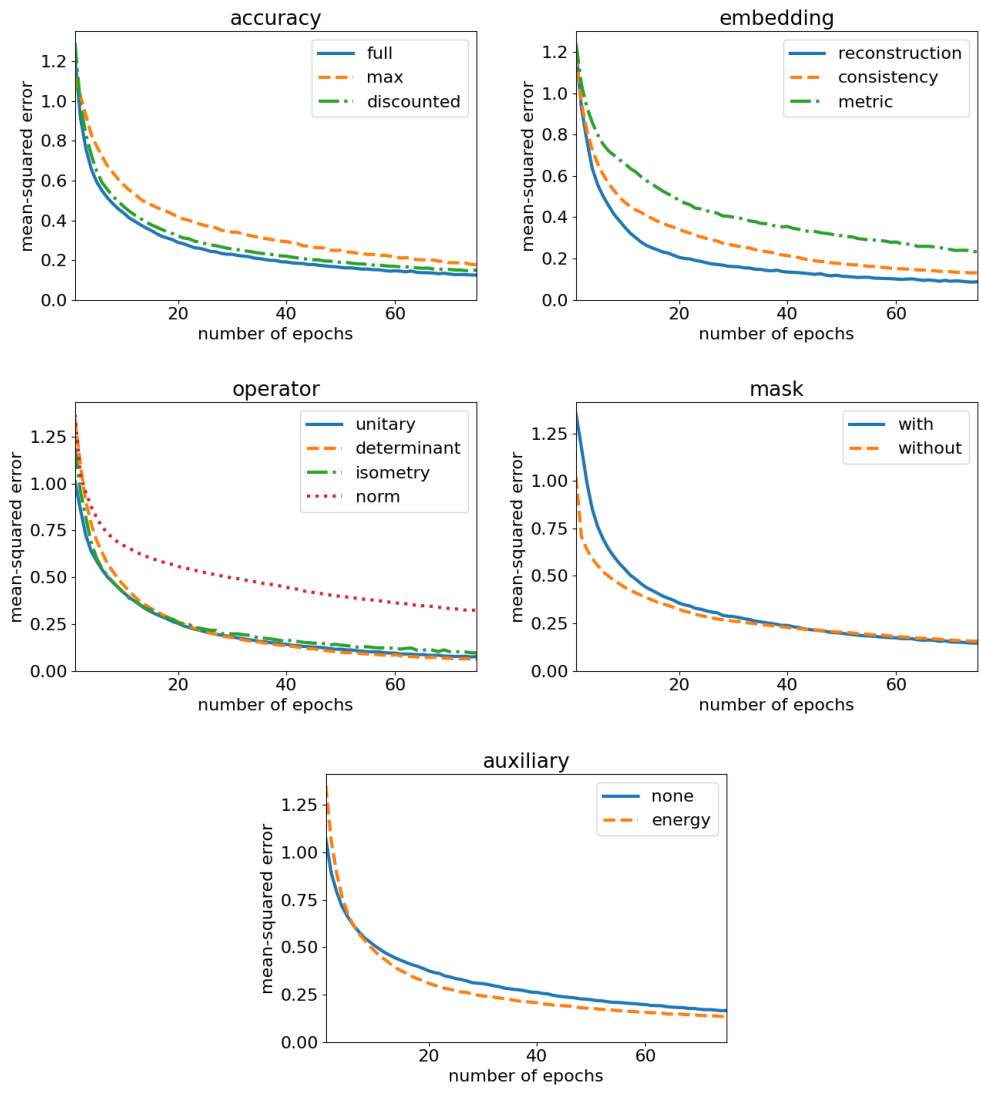


Figure 4: The mean effect of the different options of the numerical experiment for the pendulum. The top left plot compares the mean effect of the different accuracy loss terms. The top right plot compares the mean effect of the different embedding loss terms. The center left plot compares the mean effect of the different operator loss terms. The center right plot compares the mean effect of whether or not a mask is used. The bottom left plot compares the mean effect of the different auxiliary loss terms.

Table 4: The mean relative times for the numerical experiment for the pendulum.

option	mean time
full	1.947080
max	0.727518
discounted	0.325402
reconstruction	1.300984
consistency	0.946781
metric	0.752236
unitary	0.978510
determinant	1.245490
isometry	0.974475
norm	0.924270
none	1.019804
energy	0.980196
with	1.068024
without	0.909301

For the accuracy loss terms, on average, the full accuracy loss and the discounted accuracy loss performed about the same. They both performed significantly better than the maximum accuracy loss. Four of the best ten combinations used the full accuracy loss, four used the discounted accuracy loss, and two used the maximum accuracy loss.

For the embedding loss term, on average, the reconstruction loss performed the best, followed by the consistency loss and then the metric loss. All of the best ten combination used the reconstruction loss.

For the operator loss term, on average, the isometry loss, the unitary loss and the determinant loss performed similarly, and these three terms performed significantly better than the norm loss. Five of the best ten combinations used the unitary loss, three used the isometry loss and two used the determinant loss.

For the mask, on average, having a mask and not having a mask performed similarly. Seven of the top ten combinations used a mask.

For the auxiliary loss terms, on average, using the energy-conservation loss term performed slightly better than not using it. Four of the best ten combinations used the energy-conservation loss term.

Some of the same combinations of options with different embedding dimensions appeared in the best ten combinations. This demonstrates that these loss combinations are robust.

For the most part, the mean times for the options are similar. The accuracy loss term performed several factors slower than the other accuracy loss terms. The reconstruction loss performed slightly slower than the other embedding loss terms. And, the determinant loss term performed slightly slower than the other operator loss terms.

5.3 Lorenz System

In this numerical experiment, the embedding dimensions 8, 16, 32 and 64 are considered. And, the discount factors 1.0, 0.975 and 0.95 are considered. All combinations of each of the different types of loss terms of considered and whether or not the mask is used, except that the determinant loss is only considered with a mask.

In this numerical experiment, the embedding dimensions 32 and 64 were considered. Furthermore, all combinations between the accuracy loss terms, the embedding loss terms, the operator loss terms and whether or not a mask was used so that the operator is tridiagonal were considered, except that the determinant loss is only considered with a mask Thus, 144 combinations were con-

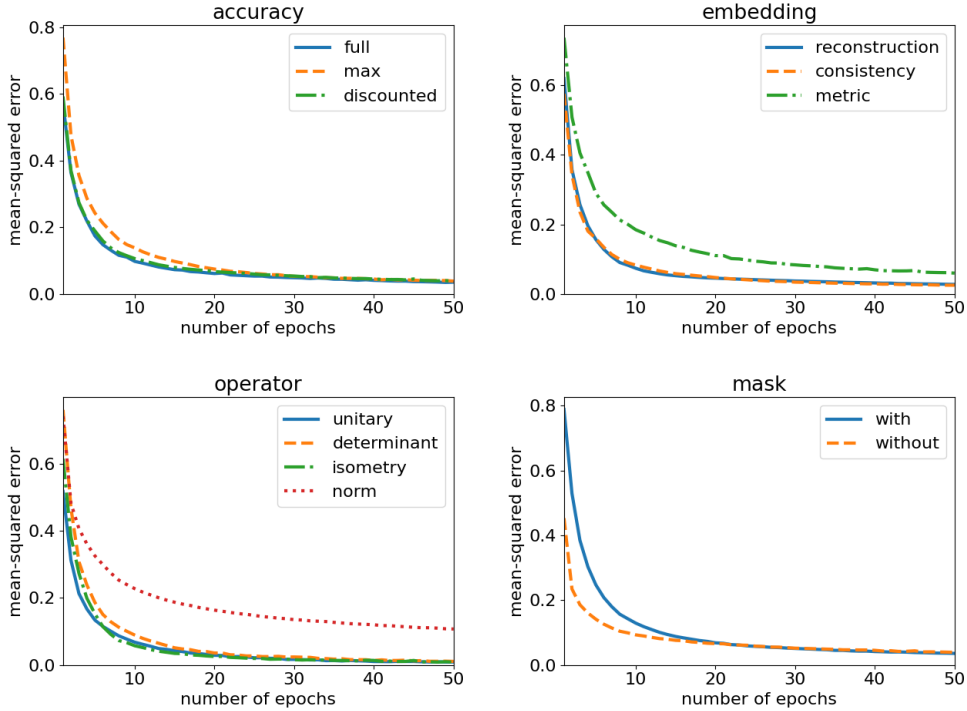


Figure 5: The mean effect of the different options of the numerical experiment for the Lorenz system. The top left plot compares the mean effect of the different accuracy loss terms. The top right plot compares the mean effect of the different embedding loss terms. The bottom left plot compares the mean effect of the different operator loss terms. The bottom right plot compares the mean effect of whether or not a mask is used.

sidered. Figure 5 shows the mean error for the different options as the number of epochs increases. Table 5 shows the ten best combinations at 30 epochs. Table 6 shows the mean relative times for the different options, that is, the mean times for the different options divided by the overall mean time. Figure 6 is direct comparisons between the embedding terms and also the operator terms.

For the accuracy loss terms, on average, all the accuracy terms performed similarly. Five of the best ten combinations used the full accuracy loss, three used the maximum accuracy loss, and two used the discounted accuracy loss.

For the embedding loss term, on average, the metric loss performed significantly worse than the reconstruction loss and the consistency loss. Seven of the best ten combinations used the reconstruction loss, and three used the consistency loss. In the direct comparison, the metric loss

Table 5: The ten best combinations for the numerical experiment for the Lorenz system at 30 epochs. The dimension is the dimension of the latent space.

error	accuracy	embedding	operator	mask	dimension
0.001249	full	reconstruction	unitary	with	64
0.001505	discounted	reconstruction	determinant	with	64
0.001605	discounted	reconstruction	unitary	with	64
0.001691	full	reconstruction	determinant	with	64
0.002287	max	reconstruction	unitary	with	64
0.002292	max	reconstruction	determinant	with	64
0.002741	full	consistency	unitary	with	64
0.002878	full	reconstruction	isometry	without	64
0.002879	full	consistency	isometry	with	64
0.002900	max	consistency	isometry	with	64

Table 6: The mean relative times for the numerical experiment for the Lorenz system.

option	mean time
full	1.859016
max	0.726902
discounted	0.414082
reconstruction	1.273235
consistency	0.895752
metric	0.831013
unitary	1.039408
determinant	1.156576
isometry	0.983032
norm	0.899272
with	1.053328
without	0.928897

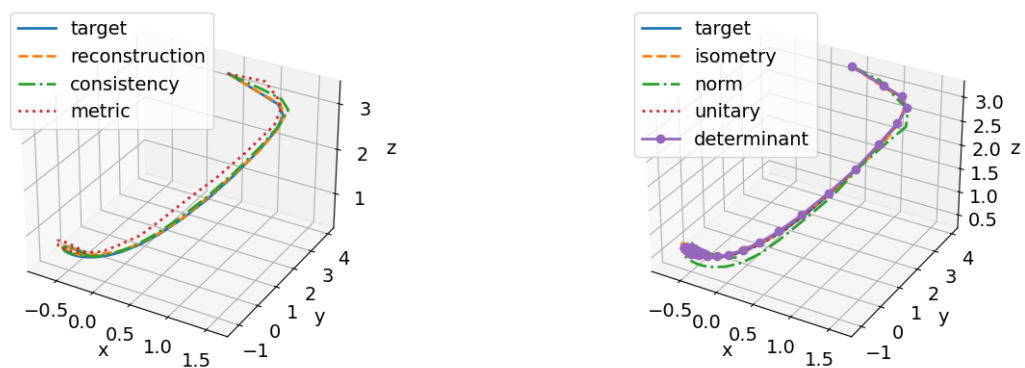


Figure 6: Direct comparison of loss terms for the Lorenz system. On the left, the embedding term is varied while the other terms are fixed. On the right, the operator term is varied while the other terms are fixed. In each comparison, the embedding dimension is 64, a mask is used, the full accuracy loss is used, and an auxiliary loss term is not used. In the comparison of the embedding terms, the unitary loss is used. In the comparison of the operator terms, the reconstruction loss is used.

does worse than the other embedding loss terms.

For the operator loss term, on average, the isometry loss, the unitary loss and the determinant loss performed similarly, and these three terms performed significantly better than the norm loss. Four of the best ten combinations used the unitary loss, three used the isometry loss and three used the determinant loss. In the direct comparison, the norm loss does worse than the other operator loss terms.

For the mask, on average, having a mask and not having a mask performed similarly. Furthermore, nine of the top ten combinations used a mask.

In all of the top ten combinations, the embedding dimension was 64. This demonstrates that the model size was more important than the options. It is likely that the other embedding dimension were too small for the Lorenz system.

For the most part, the mean times for the options are similar. The accuracy loss term performed several factors slower than the other accuracy loss terms. The reconstruction loss performed slightly slower than the other embedding loss terms. And, the determinant loss term performed slightly slower than the other operator loss terms.

5.4 Heat Equation

In this numerical experiment, the embedding dimensions 64 and 128 were considered. Furthermore, all combinations between the accuracy loss terms, the embedding loss terms, the operator loss terms, whether or not the auxiliary absolute-max loss term was used and whether or not a mask was used so that the operator is tridiagonal were considered, except that the determinant loss is only considered with a mask. Thus, 288 combinations were considered. Figure 7 shows the mean error for the different options as the number of epochs increases. Table 7 shows the ten best combinations at 20 epochs. Table 8 shows the mean relative times for the different options, that is, the mean times for the different options divided by the overall mean time.

For the accuracy loss terms, on average, all the accuracy terms performed similarly. Five of the best ten combinations used the full accuracy loss, three used the discounted accuracy loss, and two used the maximum accuracy loss.

For the embedding loss term, on average, the consistency loss performed significantly better than the metric loss and the reconstruction loss. Furthermore, all of the best ten combination used the consistency loss.

For the operator loss term, on average, the isometry loss performed significantly worse than the

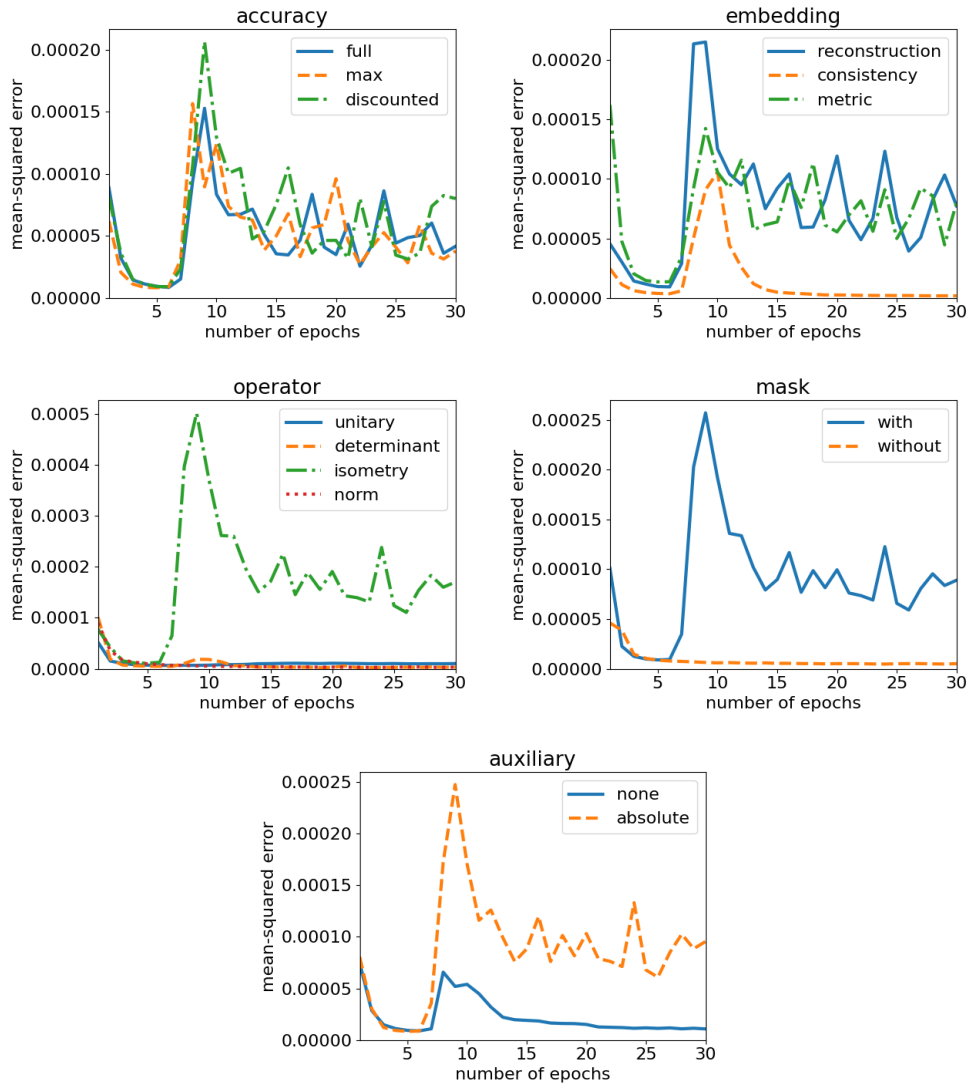


Figure 7: The mean effect of the different options of the numerical experiment for the heat equation. The top left plot compares the mean effect of the different accuracy loss terms. The top right plot compares the mean effect of the different embedding loss terms. The center left plot compares the mean effect of the different operator loss terms. The center right plot compares the mean effect of whether or not a mask is used. The bottom left plot compares the mean effect of the different auxiliary loss terms.

Table 7: The ten best combinations for the numerical experiment for the heat equation at 20. The dimension is the dimension of the latent space.

error	accuracy	embedding	operator	auxiliary	mask	dimension
1e-7	discounted	consistency	determinant	none	with	128
1e-6	full	consistency	determinant	none	with	128
1e-6	discounted	consistency	isometry	none	without	128
1e-6	full	consistency	determinant	none	with	64
1e-6	discounted	consistency	determinant	none	with	64
1e-6	max	consistency	norm	none	with	64
1e-6	full	consistency	norm	absolute	with	128
1e-6	max	consistency	determinant	absolute	with	128
1e-6	full	consistency	isometry	none	without	128
1e-7	full	consistency	isometry	none	without	64

other operator loss terms. Five of the best ten combinations used the determinant loss, three used the isometry loss and two used the norm loss.

For the mask, on average, not having as mask performed much better. But, seven of the best ten combinations used a mask.

Some of the same combinations of options with different embedding dimensions appeared in the best ten combinations. This demonstrates that these loss combinations are robust.

For the most part, the mean times for the options are similar. The determinant loss term performed slightly slower than the other operator loss terms.

5.5 Wave Equation

In this numerical experiment, the embedding dimensions 256 was considered. Furthermore, all combinations between the accuracy loss terms, the embedding loss terms, the operator loss terms, whether or not the absolute max loss was used and whether or not a mask was used so that the operator is tridiagonal were considered, except that the determinant loss is only considered with a mask Thus, 288 combinations were considered. Figure 8 shows the mean error for the different options as the number of epochs increases. Table 9 shows the ten best combinations at 30 epochs.

Table 8: The mean relative times for the numerical experiment for the heat equation.

option	mean time
full	0.979201
max	1.003339
discounted	1.017461
reconstruction	1.100878
consistency	0.989917
metric	0.909205
unitary	0.957837
determinant	1.193389
isometry	0.962771
norm	0.982697
none	0.994160
absolute	1.005840
with	1.035062
without	0.953251

Table 9: The ten best combinations for the numerical experiment with the wave equation at 30 epochs. The dimension is the dimension of the latent space.

error	accuracy	embedding	operator	auxiliary	mask	dimension
0.004519	discounted	reconstruction	unitary	none	with	256
0.004697	full	consistency	isometry	none	with	256
0.005081	full	reconstruction	unitary	none	with	256
0.005167	discounted	consistency	determinant	none	with	128
0.005582	full	consistency	unitary	none	with	256
0.005680	full	reconstruction	unitary	none	with	128
0.005806	discounted	consistency	unitary	none	with	256
0.005870	discounted	reconstruction	unitary	none	with	128
0.005918	discounted	consistency	unitary	none	with	128
0.005954	full	reconstruction	determinant	none	with	256

Table 10 shows the mean relative times for the different options, that is, the mean times for the different options divided by the overall mean time. Figure 9 is direct comparisons between the embedding terms and also the operator terms.

For the accuracy loss terms, on average, the full accuracy loss and the discounted accuracy loss performed about the same. They both performed significantly better than the maximum accuracy loss. Five of the best ten combinations used the full accuracy loss, and five used the discounted accuracy loss.

For the embedding loss term, on average, the consistency loss performed the best, followed by the reconstruction loss and then the metric loss. Five of the best ten combinations used the consistency loss, and five used the reconstruction loss.

For the operator loss term, on average, the determinant loss performed the best, followed by the isometry loss and unitary loss, and then the norm loss. Seven of the best ten combinations used the unitary loss, two used the determinant loss, and one used the isometry loss. In the direct comparison, the norm loss performed worse than the other operator loss terms, and the determinant loss performed the best.

For the auxiliary loss terms, on average, using or not using the absolute maximum loss performed

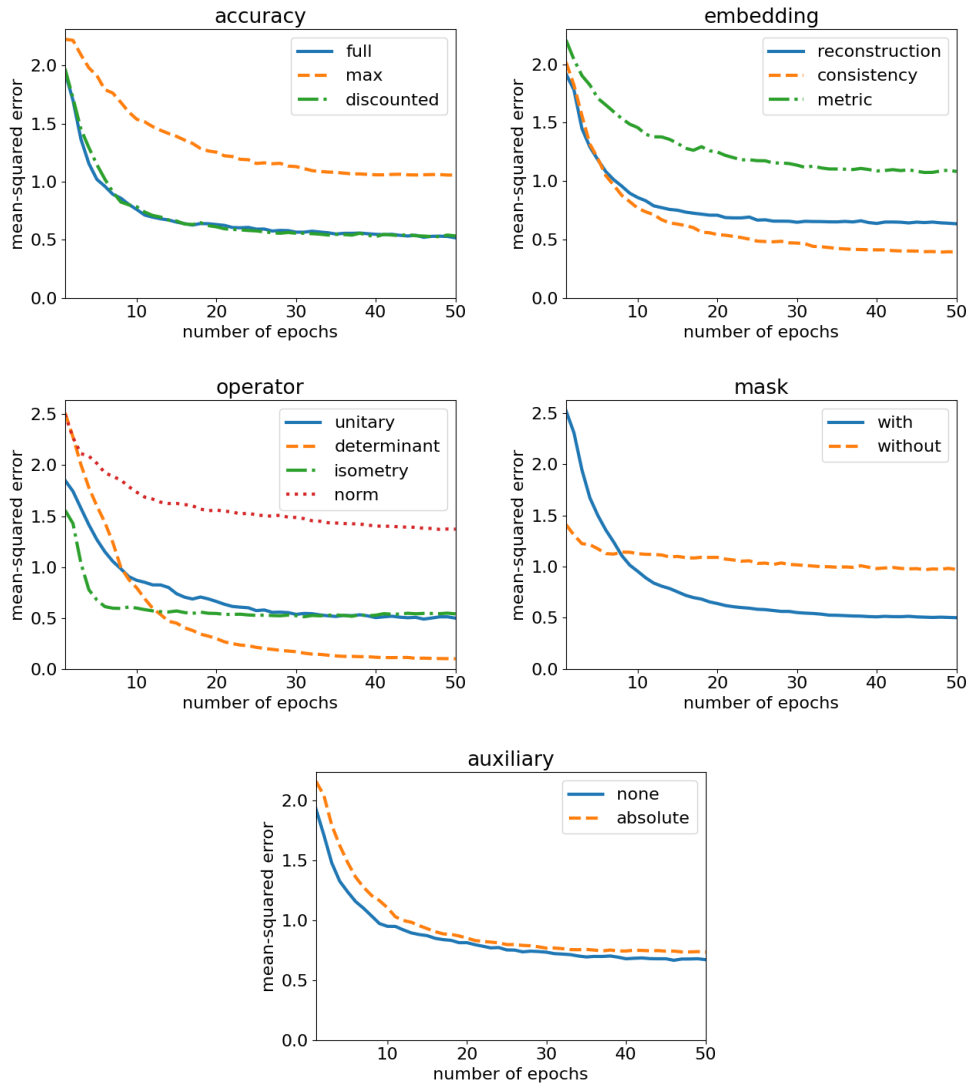


Figure 8: The mean effect of the different options of the numerical experiment for the wave equation. The top left plot compares the mean effect of the different accuracy loss terms. The top right plot compares the mean effect of the different embedding loss terms. The center left plot compares the mean effect of the different operator loss terms. The center right plot compares the mean effect of whether or not a mask is used. The bottom left plot compares the mean effect of the different auxiliary loss terms.

Table 10: The mean relative times for the numerical experiment for the wave equation.

option	mean time
full	1.018608
max	1.005451
discounted	0.975941
reconstruction	1.088658
consistency	0.985603
metric	0.925739
unitary	0.922116
determinant	1.321372
isometry	0.894227
norm	1.022971
none	0.997791
absolute	1.002209
with	1.084602
without	0.887197

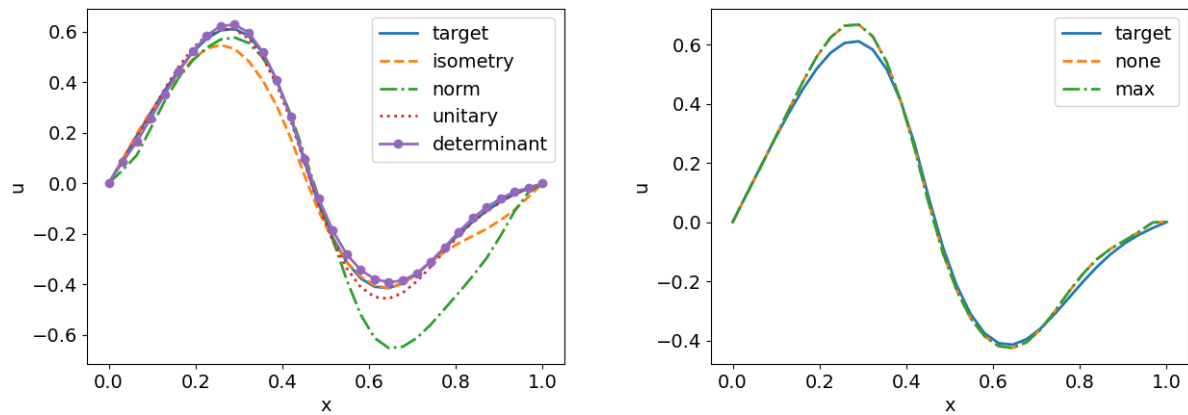


Figure 9: Direct comparison of loss terms for the wave equation. Each plot is a time slice of the solution at a time later than the start time. On the left, the operator term is varied while the other terms are fixed. On the right, the auxiliary term is varied while the other terms are fixed. In each comparison, the embedding dimension is 64, a mask is used, the full accuracy loss is used, and the reconstruction loss is used. In the comparison of the operator terms, an auxiliary loss term is not used. In the comparison of the auxiliary loss term, the unitary loss is used.

similarly. But, all of the best ten combinations did not use an auxiliary loss term. In the direct comparison, using or not using the absolute maximum loss performed similarly.

For the mask, on average, having a mask performed better. Furthermore, all of the top ten combinations used a mask.

Some of the same combinations of options with different embedding dimensions appeared in the best ten combinations. This demonstrates that these loss combinations are robust.

For the most part, the mean times for the options are similar. The determinant loss term performed slightly slower than the other operator loss terms.

5.6 Burger's Equation

In this numerical experiment, the embedding dimensions 512 and 1024 were considered. Furthermore, all combinations between the accuracy loss terms, the embedding loss terms, the operator loss terms, whether or not the auxiliary absolute-max loss term was used and whether or not a mask was used so that the operator is tridiagonal were considered, except that the determinant loss is only considered with a mask. Thus, 288 combinations were considered. Figure 10 shows the mean error for the different options as the number of epochs increases. Table 11 shows the ten best combinations at 50 epochs. Table 12 shows the mean relative times for the different options, that is, the mean times for the different options divided by the overall mean time. Figure 11 is direct comparisons between the embedding terms and also the operator terms.

For the accuracy loss terms, on average, the full accuracy loss and the discounted accuracy loss performed about the same. They both performed slightly better than the maximum accuracy loss. Seven of the best ten combinations used the full accuracy loss, and three used the discounted accuracy loss.

For the embedding loss term, on average, the reconstruction loss performed the best, followed by the consistency loss and then the metric loss. Eight of the best ten combinations used the consistency loss, and two used the reconstruction loss. In the direct comparison, the reconstruction loss performed the best.

For the operator loss term, on average, the determinant loss performed the best, followed by the isometry loss and unitary loss, and then the norm loss. Four of the best ten combinations used the unitary loss, three used the determinant loss, and three used the isometry loss. In the direct comparison, the unitary loss and determinant loss performed better than the isometry loss and the norm loss.

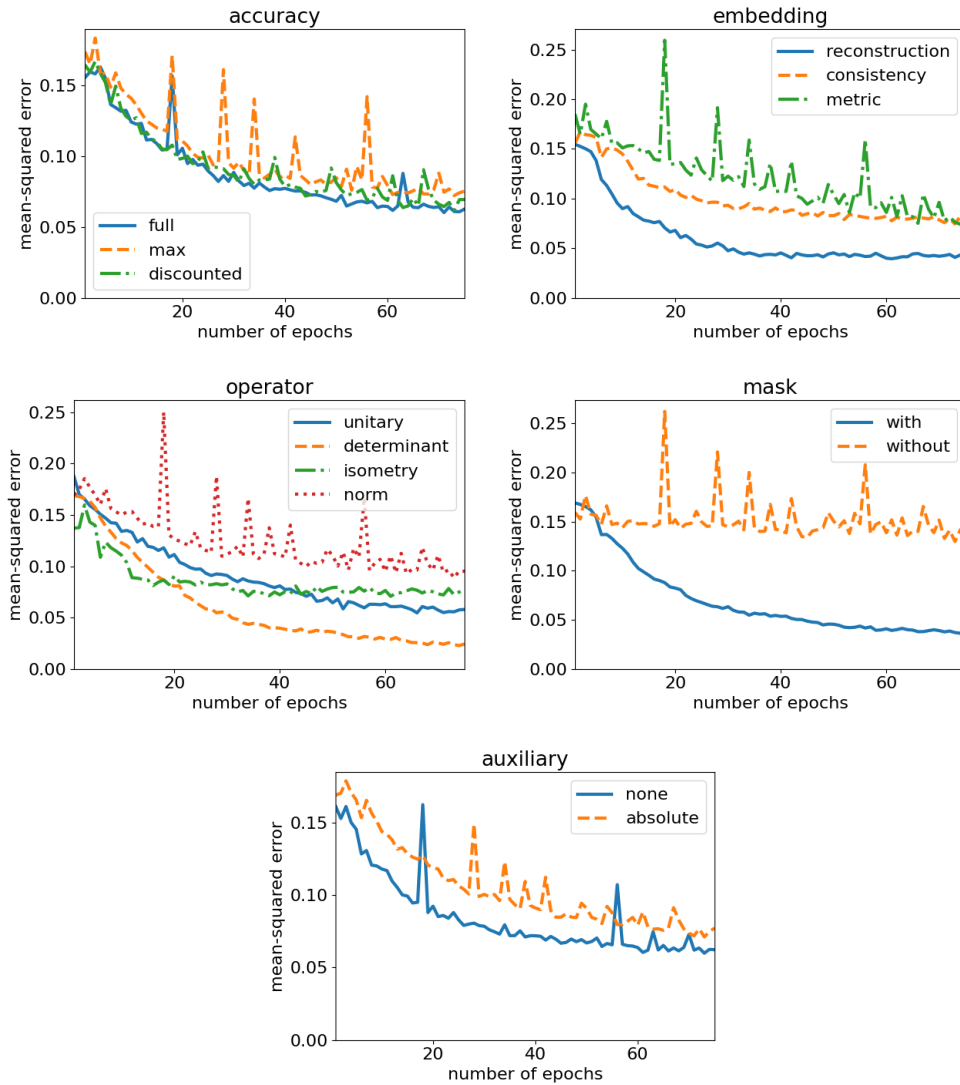


Figure 10: The mean effect of the different options of the numerical experiment for Burger’s equation. The top left plot compares the mean effect of the different accuracy loss terms. The top right plot compares the mean effect of the different embedding loss terms. The center left plot compares the mean effect of the different operator loss terms. The center right plot compares the mean effect of whether or not a mask is used. The bottom left plot compares the mean effect of the different auxiliary loss terms.

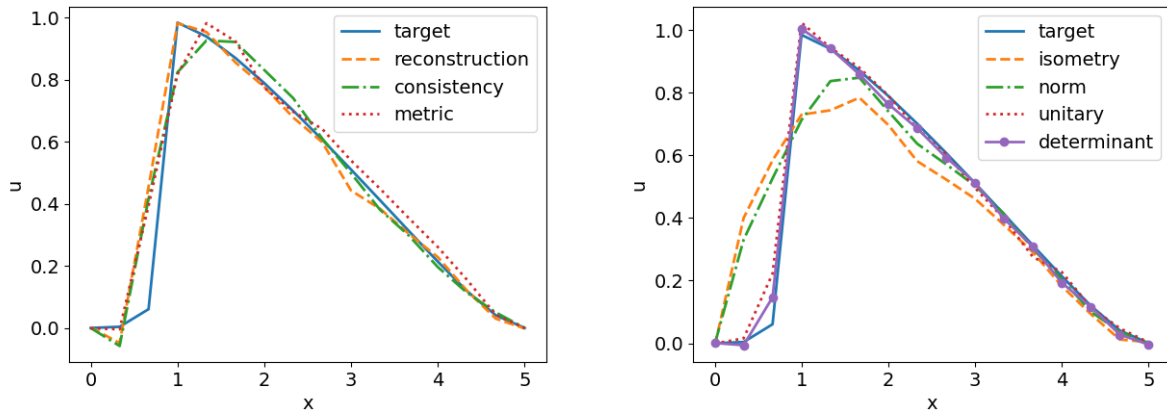


Figure 11: Direct comparison of loss terms for Burger’s equation. Each plot is a time slice of the solution at a time later than the start time. On the left, the embedding term is varied while the other terms are fixed. On the right, the operator term is varied while the other terms are fixed. In each comparison, the embedding dimension is 64, a mask is used, the full accuracy loss is used, and an auxiliary loss term is not used. In the comparison of the embedding terms, the unitary loss is used. In the comparison of the operator terms, the reconstruction loss is used.

Table 11: The ten best combinations for the numerical experiment for Burger’s equation motion at 50 epochs. The dimension is the dimension of the latent space.

error	accuracy	embedding	operator	auxiliary	mask	dimension
0.002115	full	consistency	unitary	none	with	512
0.002416	full	reconstruction	unitary	none	with	512
0.002751	full	consistency	isometry	none	with	512
0.002813	full	reconstruction	determinant	none	with	512
0.003033	full	consistency	determinant	none	with	512
0.003074	discounted	consistency	unitary	none	with	512
0.003309	discounted	consistency	isometry	none	with	512
0.003746	discounted	consistency	determinant	none	with	512
0.004211	full	consistency	unitary	none	with	1024
0.004310	max	consistency	isometry	none	with	512

For the auxiliary loss terms, on average, not using the absolute maximum loss performed better. Furthermore, all of the best ten combinations did not use an auxiliary loss term.

For the mask, on average, having a mask performed better. Furthermore, all of the top ten combinations used a mask.

Only one combination of options was repeated in the best ten combinations. And, it was the only best ten combination that did not use the 512 for the embedding dimension. The embedding dimension 1024 may have been too big for such an early epoch.

For the most part, the mean times for the options are similar. The unitary loss performed slightly slower than the other operator loss terms by over a factor of 2.

5.7 Conclusion

The full accuracy loss is the most robust accuracy loss term, and it is recommend. If the model is obviously struggling with initial learning, then it may be beneficial to try the discounted accuracy loss.

The reconstruction loss and the consistency loss performed similarly overall. One did better for

Table 12: The mean relative times for the numerical experiment for Burger's equations.

option	mean time
full	0.996650
max	0.997402
discounted	1.005948
reconstruction	1.030242
consistency	0.987900
metric	0.981858
unitary	2.283492
determinant	0.987301
isometry	0.361504
norm	0.361354
none	0.999075
absolute	1.000925
with	0.999741
without	1.000345

some equations, and the other did better for other equations. It may be beneficial to try both of these terms in practice. But, either term is probably safe to use.

The tridiagonal operator was more robust than the dense operator. The unitary loss and the determinant loss are the most robust operator loss terms. The operator form and loss term is further studied in the next section.

Overall the auxiliary loss terms did not increase performance significantly. It is not normally recommended to use them. But, for some systems, it may be beneficial to experiment with a physics-informed loss term that is specific to the system.

In each experiment, the speeds of each option were similar. The differences in speed do not seem significant enough to be a factor in choosing the loss functions.

The biggest differences were that the reconstruction loss was slightly slower than the other encoder loss terms and that the determinant loss was slightly slower than the other operator loss terms. Intuitively, it makes sense that the reconstruction loss is slower than the other encoder loss terms because it requires the most additional computations. In these experiments, the reconstruction loss was trained using the data at each time step. But, in the prediction of many time steps, it might be reasonable to train it on less data to reduce the computational cost.

The determinant loss was slower than the other operator loss terms. Intuitively, it is slower because it cannot be parallelized. But, it scales linearly, and this should not become a problem with any model size.

In these experiments, the operator was a dense matrix in the backend computations. But, a custom layer could be created for the tridiagonal form. Then, multiplication can be defined on this layer so that it scales linearly with the dimension.

6 Loss for and Form of the Operator

The experiments in this section compare the loss terms for and operator forms for Koopman autoencoders. Unlike the experiments in the previous section, these experiments are for many epochs. For the experiments in this section, the full accuracy loss and the reconstruction loss are used because these were demonstrated to be the most robust in the previous section. Furthermore, other than possibly an operator loss term, another loss term is not used. Furthermore, because the previous section already studied the times for various loss terms, this is not studied in this section.

For each equation, all combinations between the operator forms and operator loss terms are

considered, expect that the determinant loss is not considered with the dense operator form. Furthermore, unlike in the previous section, the possibility of not using an operator loss term is included.

6.1 Numerical Experiments

Table 13 is the results for the equation for the pendulum. The most accurate combination was the tridiagonal form with the unitary loss. The tridiagonal form of the operator was demonstrated to be the most robust form.

Table 13: Results for the pendulum

error	operator form	operator loss
1.66353e-3	dense	none
6.6002e-4	dense	isometry
6.31303e-2	dense	norm
1.89346e-2	dense	unitary
3.8495e-4	tridiagonal	none
7.4554e-4	tridiagonal	isometry
4.59331e-4	tridiagonal	norm
1.2317e-4	tridiagonal	unitary
3.8344e-4	tridiagonal	determinant
1.55339e-1	jordan	none
2.63119e-4	jordan	isometry
1.96144e-2	jordan	norm
2.5279e-2	jordan	unitary
2.42197e-1	jordan	determinant

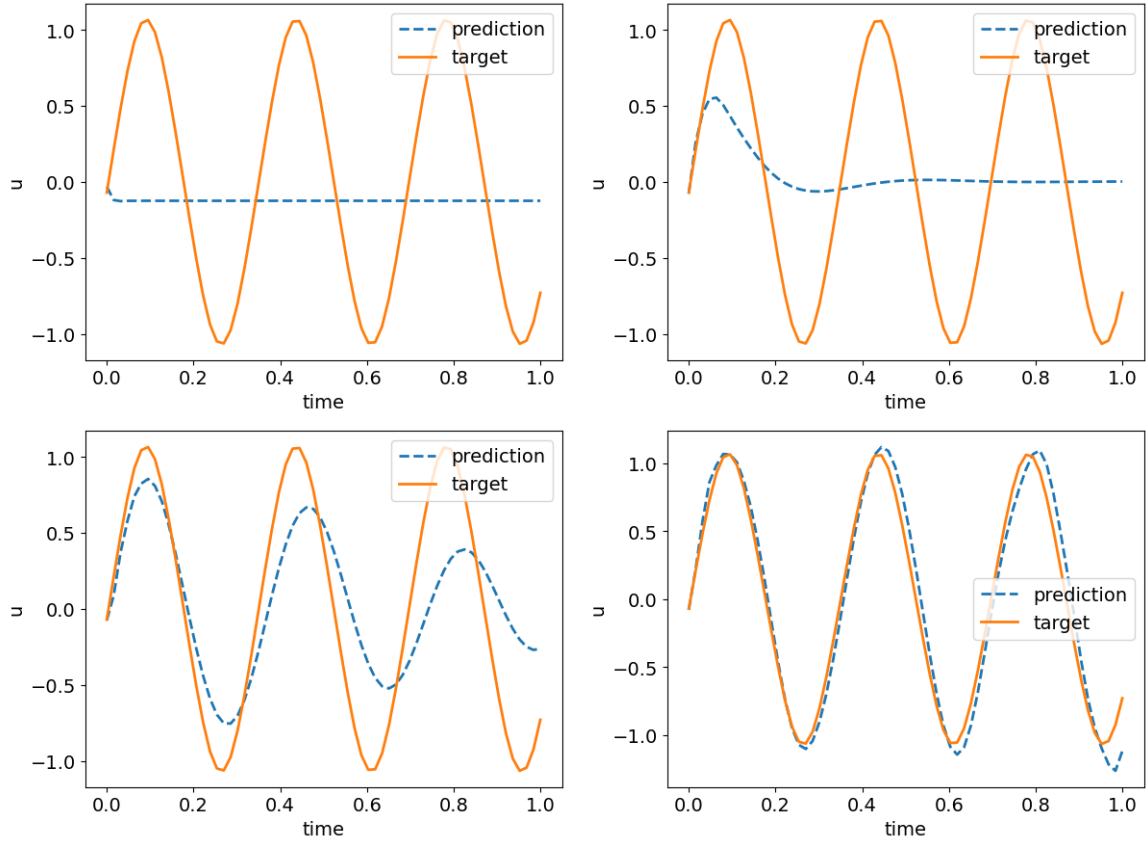


Figure 12: Progress learning the equation for the pendulum: The model uses the tridiagonal form of the operator and the determinant loss. The frames are at 1, 10, 50, and 200 epochs. The scales are normalized.

Table 14 is the results for the equation for the pendulum. The most accurate combination was the Jordan form without an operator loss term. Unlike the other experiments, the lack of an operator loss term does well.

Table 14: Results for the Lorenz system

error	operator form	operator loss
7.312e-3	dense	none
1.390e-2	dense	isometry
8.495e-2	dense	norm
1.342e-2	dense	unitary
6.368e-3	tridiagonal	none
1.586e-2	tridiagonal	isometry
1.182e-1	tridiagonal	norm
7.386e-3	tridiagonal	unitary
6.679e-3	tridiagonal	determinant
2.114e-3	jordan	none
5.266e-3	jordan	isometry
3.989e-2	jordan	norm
8.151e-3	jordan	unitary
1.961e-2	jordan	determinant

Table 15 is the results for the equation for the fluid attractor equation. The most accurate combination was the tridiagonal form with the determinant loss. The tridiagonal form of the operator was demonstrated to be the most robust form.

Table 15: Results for the fluid attractor equation

error	operator form	operator loss
2.47e-6	dense	none
7.02e-5	dense	isometry
1.30e-2	dense	norm
1.040e-5	dense	unitary
3.79e-6	tridiagonal	none
2.52e-5	tridiagonal	isometry
1.80e-2	tridiagonal	norm
3.69e-6	tridiagonal	unitary
1.99e-6	tridiagonal	determinant
2.020e-2	jordan	none
2.08e-5	jordan	isometry
1.67e-2	jordan	norm
7.05e-6	jordan	unitary
2.20e-2	jordan	determinant

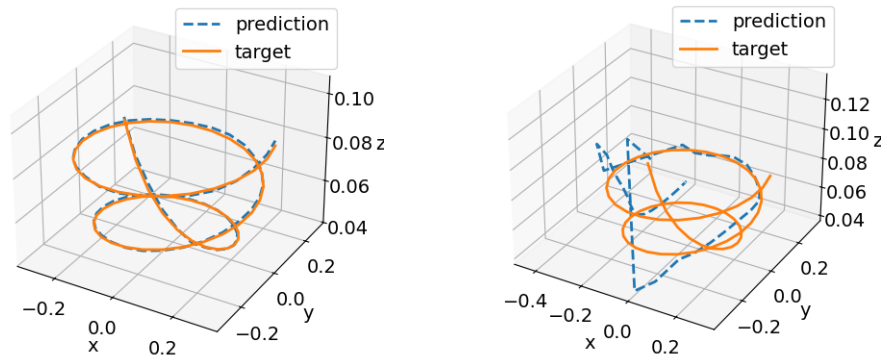


Figure 13: Comparison of two operator loss terms for the fluid attractor equation: Both plots are of the trajectories of the target and the prediction. On the left, the model uses the tridiagonal form of the operator and the determinant loss. On the right, the model uses the dense form of the operator and the norm loss. These predictions are at 2000 epochs.

Table 16 is the results for the equation for the fluid attractor equation. The most accurate combination was the tridiagonal form without an unitary loss. The tridiagonal form of the operator was demonstrated to be the most robust form.

Table 16: Results for Burger's equation

error	operator form	operator loss
3.269e-3	dense	none
4.753e-3	dense	isometry
3.048e-2	dense	norm
2.824e-3	dense	unitary
1.234e-3	tridiagonal	none
3.666e-3	tridiagonal	isometry
1.998e-2	tridiagonal	norm
1.375e-3	tridiagonal	unitary
1.703e-3	tridiagonal	determinant
2.470e-2	jordan	none
2.082e-3	jordan	isometry
2.20952e-2	jordan	norm
2.268e-3	jordan	unitary
2.1471e-2	jordan	determinant

Table 17 is the results for the equation for the fluid attractor equation. The most accurate combination was the tridiagonal form with the unitary loss. The tridiagonal form of the operator was demonstrated to be the most robust form.

Table 17: Results for the KdV equation

error	operator form	operator loss
2.531e-1	dense	none
3.164e-1	dense	isometry
1.699e-1	dense	norm
2.838e-2	dense	unitary
1.579e-1	tridiagonal	none
2.410e-1	tridiagonal	isometry
7.294e-1	tridiagonal	norm
4.467e-2	tridiagonal	unitary
4.807e-2	tridiagonal	determinant
1.421e-1	jordan	none
1.254	jordan	isometry
1.012e-1	jordan	norm
9.378e-1	jordan	unitary
5.0974e-1	jordan	determinant

6.2 Conclusion

The best combination varied from equation to equation. Overall, the tridiagonal form of the operator is the most robust. Furthermore, the unitary loss term was the most robust operator loss term. It is recommended to use the tridiagonal form with the unitary loss term.

7 Conclusion

The full accuracy loss term is the most robust accuracy loss term. The reconstruction loss term and the consistency loss terms are the most robust encoding loss terms. The tridiagonal form of the operator is the most robust operator form. And, the unitary loss term is the most robust operator loss term. It is recommended to use the full accuracy loss term, the reconstruction loss term, and the unitary loss term with the tridiagonal form of the operator.

Code Availability

The code for the numerical experiments is publicly available at https://gitlab.com/dustin_lee/neural-operators. All experiments were done in Python. Neural networks were implemented with PyTorch [55–57] and Lightning [58]. Hyperparameter configuration was done using Hydra [59].

Declaration of Competing Interest

The authors declare that they have no known competing financial interests or personal relationships that could have appeared to influence the work reported in this paper.

Acknowledgments

Guang Lin would like to thank the support of the National Science Foundation (DMS-2053746, DMS-2134209, ECCS-2328241, CBET-2347401 and OAC-2311848), and U.S. Department of Energy (DOE) Office of Science Advanced Scientific Computing Research program DE-SC0023161, and DOE–Fusion Energy Science, under grant number: DE-SC0024583.

References

- [1] Nikola B Kovachki, Samuel Lanthaler, and Andrew M Stuart. “Operator learning: Algorithms and analysis”. In: *arXiv preprint arXiv:2402.15715* (2024).
- [2] Nicolas Boullé and Alex Townsend. “A mathematical guide to operator learning”. In: *arXiv preprint arXiv:2312.14688* (2023).
- [3] Nick Winovich. “Neural Network Approximations to Solution Operators for Partial Differential Equations”. PhD thesis. Purdue University, 2021.
- [4] Nishaal Parmar, Hazem H Refai, and Thordur Runolfsson. “A survey on the methods and results of data-driven koopman analysis in the visualization of dynamical systems”. In: *IEEE Transactions on Big Data* 8.3 (2020), pp. 723–738.
- [5] Giorgos Mamakoukas, Ian Abraham, and Todd D Murphey. “Learning data-driven stable Koopman operators”. In: *Free radical biology & medicine*. (2020).

- [6] Bowen Huang, Xu Ma, and Umesh Vaidya. “Data-driven nonlinear stabilization using koopman operator”. In: *The Koopman Operator in Systems and Control: Concepts, Methodologies, and Applications* (2020), pp. 313–334.
- [7] Stefan Klus et al. “Data-driven approximation of the Koopman generator: Model reduction, system identification, and control”. In: *Physica D: Nonlinear Phenomena* 406 (2020), p. 132416.
- [8] Steven L Brunton et al. “Koopman invariant subspaces and finite linear representations of nonlinear dynamical systems for control”. In: *PloS one* 11.2 (2016), e0150171.
- [9] Marko Budišić, Ryan Mohr, and Igor Mezić. “Applied koopmanism”. In: *Chaos: An Interdisciplinary Journal of Nonlinear Science* 22.4 (2012).
- [10] J Nathan Kutz, Xing Fu, and Steven L Brunton. “Multiresolution dynamic mode decomposition”. In: *SIAM Journal on Applied Dynamical Systems* 15.2 (2016), pp. 713–735.
- [11] Naoya Takeishi, Yoshinobu Kawahara, and Takehisa Yairi. “Learning Koopman invariant subspaces for dynamic mode decomposition”. In: *Advances in neural information processing systems* 30 (2017).
- [12] M Budišić, R Mohr, and I Mezić. *The Koopman Operator in Systems and Control: Concepts, Methodologies, and Applications*. 2020.
- [13] Yunzhu Li et al. “Learning compositional koopman operators for model-based control”. In: *arXiv preprint arXiv:1910.08264* (2019).
- [14] Eurika Kaiser, J Nathan Kutz, and Steven L Brunton. “Data-driven approximations of dynamical systems operators for control”. In: *The Koopman Operator in Systems and Control: Concepts, Methodologies, and Applications* (2020), pp. 197–234.
- [15] Yiqiang Han, Wenjian Hao, and Umesh Vaidya. “Deep learning of Koopman representation for control”. In: *2020 59th IEEE Conference on Decision and Control (CDC)*. IEEE. 2020, pp. 1890–1895.
- [16] Daniel Bruder et al. “Koopman-based control of a soft continuum manipulator under variable loading conditions”. In: *IEEE robotics and automation letters* 6.4 (2021), pp. 6852–6859.
- [17] Daniel Bruder et al. “Modeling and control of soft robots using the koopman operator and model predictive control”. In: *arXiv preprint arXiv:1902.02827* (2019).

- [18] Hassan Arbabi, Milan Korda, and Igor Mezić. “A data-driven koopman model predictive control framework for nonlinear partial differential equations”. In: *2018 IEEE Conference on Decision and Control (CDC)*. IEEE. 2018, pp. 6409–6414.
- [19] Ian Abraham, Gerardo De La Torre, and Todd D Murphey. “Model-based control using Koopman operators”. In: *arXiv preprint arXiv:1709.01568* (2017).
- [20] Lu Lu et al. “Learning nonlinear operators via DeepONet based on the universal approximation theorem of operators”. In: *Nature Machine Intelligence* 3.3 (Mar. 2021), pp. 218–229. ISSN: 2522-5839. DOI: 10.1038/s42256-021-00302-5. URL: <http://dx.doi.org/10.1038/s42256-021-00302-5>.
- [21] Samuel Lanthaler, Siddhartha Mishra, and George E Karniadakis. “Error estimates for deep-onets: A deep learning framework in infinite dimensions”. In: *Transactions of Mathematics and Its Applications* 6.1 (2022), tnac001.
- [22] Somdatta Goswami et al. “A physics-informed variational DeepONet for predicting crack path in quasi-brittle materials”. In: *Computer Methods in Applied Mechanics and Engineering* 391 (2022), p. 114587.
- [23] Junyan He et al. “Novel DeepONet architecture to predict stresses in elastoplastic structures with variable complex geometries and loads”. In: *Computer Methods in Applied Mechanics and Engineering* 415 (2023), p. 116277.
- [24] Sung Woong Cho, Jae Yong Lee, and Hyung Ju Hwang. “Learning time-dependent PDE via graph neural networks and deep operator network for robust accuracy on irregular grids”. In: *arXiv preprint arXiv:2402.08187* (2024).
- [25] Lu Lu et al. “A comprehensive and fair comparison of two neural operators (with practical extensions) based on fair data”. In: *Computer Methods in Applied Mechanics and Engineering* 393 (2022), p. 114778.
- [26] Zongyi Li et al. “Fourier neural operator for parametric partial differential equations”. In: *arXiv preprint arXiv:2010.08895* (2020).
- [27] Shaoxiang Qin et al. “Toward a Better Understanding of Fourier Neural Operators: Analysis and Improvement from a Spectral Perspective”. In: *arXiv preprint arXiv:2404.07200* (2024).
- [28] Zongyi Li et al. “Fourier neural operator with learned deformations for pdes on general geometries”. In: *Journal of Machine Learning Research* 24.388 (2023), pp. 1–26.

- [29] Johannes Brandstetter, Max Welling, and Daniel E Worrall. “Lie point symmetry data augmentation for neural PDE solvers”. In: *International Conference on Machine Learning*. PMLR. 2022, pp. 2241–2256.
- [30] Nikola Kovachki, Samuel Lanthaler, and Siddhartha Mishra. “On universal approximation and error bounds for Fourier neural operators”. In: *Journal of Machine Learning Research* 22.290 (2021), pp. 1–76.
- [31] Alasdair Tran et al. “Factorized fourier neural operators”. In: *arXiv preprint arXiv:2111.13802* (2021).
- [32] Matthew Tancik et al. “Fourier features let networks learn high frequency functions in low dimensional domains”. In: *Advances in neural information processing systems* 33 (2020), pp. 7537–7547.
- [33] Bernard O Koopman. “Hamiltonian systems and transformation in Hilbert space”. In: *Proceedings of the National Academy of Sciences* 17.5 (1931), pp. 315–318.
- [34] Steven L Brunton et al. “Modern Koopman theory for dynamical systems”. In: *arXiv preprint arXiv:2102.12086* (2021).
- [35] Adam L Bruce, Vera M Zeidan, and Dennis S Bernstein. “What is the Koopman operator? a simplified treatment for discrete-time systems”. In: *2019 American Control Conference (ACC)*. IEEE. 2019, pp. 1912–1917.
- [36] Michael A Morrison. *Understanding quantum physics: A user’s manual*. 1990.
- [37] Hans C. Ohanian. *Principles of Quantum Mechanics*. 1989.
- [38] David J. Griffiths. *Introduction to Quantum Mechanics*. 2018.
- [39] Bethany Lusch, J Nathan Kutz, and Steven L Brunton. “Deep learning for universal linear embeddings of nonlinear dynamics”. In: *Nature communications* 9.1 (2018), p. 4950.
- [40] Haojie Shi and Max Q-H Meng. “Deep Koopman operator with control for nonlinear systems”. In: *IEEE Robotics and Automation Letters* 7.3 (2022), pp. 7700–7707.
- [41] P. Winder. *Reinforcement Learning: Industrial Applications of Intelligent Agents*. O’Reilly Media, Incorporated, 2020. ISBN: 9781098114831. URL: <https://books.google.com/books?id=u87AzQEACAAJ>.
- [42] Mengnan Li and Lijian Jiang. “Deep learning nonlinear multiscale dynamic problems using Koopman operator”. In: *Journal of Computational Physics* 446 (2021), p. 110660.

- [43] Abdolvahhab Rostamijavanani, Shanwu Li, and Yongchao Yang. “A study on data-driven identification and representation of nonlinear dynamical systems with a physics-integrated deep learning approach: Koopman operators and nonlinear normal modes”. In: *Communications in Nonlinear Science and Numerical Simulation* 123 (2023), p. 107278.
- [44] Charles R Johnson and Roger A Horn. *Matrix analysis*. Cambridge university press Cambridge, 1985.
- [45] Mohammad Khosravi. “Representer theorem for learning Koopman operators”. In: *IEEE Transactions on Automatic Control* (2023).
- [46] Lloyd N Trefethen and David Bau. *Numerical linear algebra*. SIAM, 2022.
- [47] Omri Azencot et al. “Forecasting sequential data using consistent koopman autoencoders”. In: *International Conference on Machine Learning*. PMLR, 2020, pp. 475–485.
- [48] Yuying Liu et al. “Physics-Informed Koopman Network for time-series prediction of dynamical systems”. In: *ICLR 2024 Workshop on AI4DifferentialEquations In Science*. 2024.
- [49] Julian Rice, Wenwei Xu, and Andrew August. “Analyzing Koopman approaches to physics-informed machine learning for long-term sea-surface temperature forecasting”. In: *arXiv preprint arXiv:2010.00399* (2020).
- [50] Randall J LeVeque. *Finite difference methods for ordinary and partial differential equations: steady-state and time-dependent problems*. SIAM, 2007.
- [51] Bernd R Noack et al. “A hierarchy of low-dimensional models for the transient and post-transient cylinder wake”. In: *Journal of Fluid Mechanics* 497 (2003), pp. 335–363.
- [52] Hans Petter Langtangen and Svein Linge. *Finite difference computing with PDEs: a modern software approach*. Springer Nature, 2017.
- [53] Randall J LeVeque and Randall J Leveque. *Numerical methods for conservation laws*. Vol. 214. Springer, 1992.
- [54] Norman J Zabusky and Martin D Kruskal. “Interaction of “solitons” in a collisionless plasma and the recurrence of initial states”. In: *Physical review letters* 15.6 (1965), p. 240.
- [55] Adam Paszke et al. “Automatic differentiation in PyTorch”. In: *NIPS-W*. 2017.
- [56] Ian Pointer. *Programming pytorch for deep learning: Creating and deploying deep learning applications*. O’Reilly Media, 2019.

- [57] Phillip Lippe. *UvA Deep Learning Tutorials*. <https://uvadlc-notebooks.readthedocs.io/en/latest/>. 2024.
- [58] *Torch Lightning*. URL: <https://github.com/Lightning-AI/pytorch-lightning>.
- [59] Omry Yadan. *Hydra - A framework for elegantly configuring complex applications*. Github. 2019. URL: <https://github.com/facebookresearch/hydra>.